ELSEVIER

Physica D 132 (1999) 325–338

PHYSICA D

www.elsevier.com/locate/physd

Type-II intermittency in the driven Double Scroll Circuit

Murilo S. Baptista[1,*], Iberê L. Caldas

Institute of Physics, University of Sao Paulo, C.P. 66318, CEP 05315-970, Sao Paulo, S.P., Brazil

Received 20 October 1998; received in revised form 15 February 1999; accepted 18 February 1999
Communicated by Y. Kuramoto

Abstract

In this work, we show experimental evidences, confirmed by numerical results, from type-II intermittency in the driven Double Scroll Circuit. Numerically, we found a new scaling power law dependence on the critical parameter. This result is a consequence of the new global bifurcation scenario for the T^2 torus breakdown observed in this system: a homoclinic saddle connection is the nonlinear mechanism responsible for the reinjection of the trajectory around a repelling focus. In fact, in this global scenario the total laminar phase is the spiraling laminar period (usually considered) plus the time the trajectory spends in the vicinity of the saddle points. ©1999 Elsevier Science B.V. All rights reserved.

Keywords: Chaos; Type-II intermittency; Homoclinic bifurcation

1. Introduction

The Double Scroll Circuit [1] has been studied for its electronic simplicity and variety of non-linear phenomena. The driven versions of this circuit have been extensively investigated by many authors [2–5] who have found many bifurcation phenomena not observed in the non-perturbed circuit. In this work, although the perturbed circuit version is not the same as those used in the previous cited references, we found all phenomena observed in the other driven circuits as Hopf bifurcation, type-I and chaos–chaos intermittency, hysteresis, inverse cascades, regularity of periodic windows, quasi-periodicity, devil's staircase structures, crisis, frequency entrainment of chaos, period-adding sequence, and phase-locking. Moreover, in this work, for the first time type-II intermittency was observed in the driven Double Scroll Circuit.

Intermittency is a phenomenon related to the onset of chaotic motion. Intermittent systems behave regularly, during the laminar phase, and irregularly, during the chaotic burst, alternately. Besides, the time the system spends in the laminar phase depends on the difference $\epsilon = |p - p_c|$, where p is a parameter, in this work the amplitude or the frequency of the driven force, and p_c is the critical parameter for which intermittency appears.

* Corresponding author.
[1] Present address: University of Maryland, College Park, MD, USA.

PII: S0167-2789(99)00037-8

In a classical theoretical work about intermittencies, Pomeau and Manneville identified three possible manners the periodic motion loses its stability [6,7]. So, depending on the way the eigenvalues of the monodromy matrix cross the unit circle, we can have type-I (a real eigenvalue, $+1$), type-II (conjugate complex eigenvalues), and type-III (a real eigenvalue, -1). After this pioneer work, other types of intermittencies were found [8].

We give especial attention to the type-II intermittency that shows up after a limit cycle loses its stability by a sub-critical Hopf bifurcation, which generates an unstable focus in the origin. From a mathematical point of view a periodic motion loses its stability if the conjugate complex eigenvalues of the monodromy matrix cross the unit circle. Pomeau and Manneville conjecture that there must exist a global nonlinear mechanism that reinjects the trajectory in the vicinity of the limit cycle. To simulate this nonlinear behavior, they consider the trajectory randomly reinjected around the focus. However, they do not specify this global nonlinear bifurcation scenario.

For the determination of the laminar length for the usual type-II intermittency they supposed a random reinjection distribution in a bi-dimensional disk. If this assumption is correct, the predicted length of the laminar phase should have a scaling law $\langle n\rangle \propto \ln(1/\epsilon)$ [7]. Also, in this article, the authors numerically obtained the Lyapunov exponent σ as $\sigma \cong \epsilon^{\mu}$, with $\mu \approx 0.04$, from which laminar length is supposed to behave scaling as $\epsilon^{-\mu}$.

However, another analytical result [9] indicates that the laminar length scales as the power law $\langle n\rangle \propto \epsilon^{-\beta}$, with β given depending on the value of ϵ, in specific, whether ϵ is smaller or bigger than some critical value, $\beta = 0.5$ (like the type-I intermittency [10]), or $\beta = 1.0$, respectively. This theoretical result is derived by the integration over the space, where the laminar oscillation happens, of the reinjection probability density [11].

Once different values of ϵ leads to different scaling coefficients, β, we say that the type-II intermittency regime is a non-general bifurcation. In fact, numerical results have confirmed that type-II intermittency can have a laminar length phase described by either of the two values for β.

In [12], where Richetti et al. study a periodically driven third-order nonlinear oscillator, they find a scaling law for the laminar (spiraling) episodes that fits $\langle n\rangle \propto \epsilon^{-0.5}$. Furthermore, they show that this result agrees with the theoretical scaling law obtained assuming a one-dimensional reinjection process. In addition, in that work they argue the possibility of the existence of a homoclinic bifurcation, the global bifurcation scenario that could explain the reinjection process. However, the existence of a Shil'nikov type homoclinic trajectory [13] can only be proved if the drive is turned off, and the appearance of type-II intermittency in such system is only possible if the drive is turned on. Thus, the reinjection process, responsible for the laminar (spiraling) length, is yet an open question, as also pointed out in [14]. In [11,15], it is verified that the scaling coefficient β is 1.0.

The type-II intermittency was experimentally verified to occur in an electronic oscillator [16]. In [17], there is an inverted version of the type-II intermittency corresponding to a spiraling behavior asymptotic to the origin. In [8], a type-II intermittency coexisting with a type-I intermittency is described. In [14], a double reinjection channel that directs the trajectory to one of the two foci is presented.

In order to better characterize the type-II intermittency, we study how the average length of the laminar episodes (regular behavior) scale with the distance from the parameter V to the critical parameter V_C. As we shall see, the non-generic characteristic of the type-II intermittency, as theoretically reported in [9], is not only non-generic concerning the existence of more than one scaling coefficient that depend on ϵ, but also is non-generic concerning the existence of different types of laminar phases, which leads to the existence of different scaling laws for each one of these phases.

So, we first have to redefine what we call laminar phase.

Usually, the laminar phase is considered the spiraling evolution of the trajectory from the time when the reinjection process happens up to the chaotic burst. This spiraling behavior is caused by the existence of a stable repelling focus.

In the driven Double Scroll Circuit, there is a stable repelling focus inside a stable two-frequency torus. We can only obtain a intermittent regime when this torus is destroyed. Before that happens the two-frequency torus grows

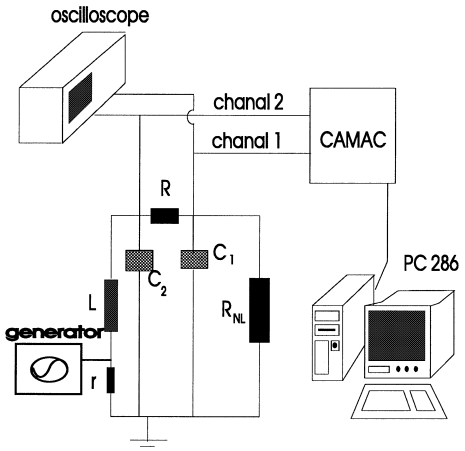

Fig. 1. The sinusoidally perturbed Double Scroll Circuit and the apparatus for the data acquisition.

in size, leading to the appearance of folds, and a homoclinic saddle connection among the saddle points [18], which is also called a homoclinic contour.

In our case, type-II intermittency is found after the homoclinic saddle connection is created, which happens after the stable two-frequency torus become unstable by a subcritical Hopf bifurcation. Thus, this global bifurcation scenario explains how the trajectory is reinjected, from the unstable manifolds of the saddle points to the unstable focus. Moreover, in addition to the regular spiraling behavior there is also a regular saddle permanence identified by the time the system spends in the vicinity of the saddle points. So, in this work, we consider as laminar phase the spiraling length, usually treated as the laminar phase of the type-II intermittency, plus the saddle permanence.

We have also found evidences that the global bifurcation scenario has a typically heteroclinic trajectory that connects the saddle points with the unstable focus.

This paper is organized as follows. In Section 2, we present the driven Double Scroll Circuit and the system of equations that simulates its dynamic. In Section 3, we show experimental observations of the type-II intermittency in this electronic circuit. For a better understanding of the experimental results, we show in Section 4, numerical results confirming the existence of the type-II intermittency transition to chaos. In this section, we also show, by analyzing the Lyapunov exponent, that the onset of chaos in this case is abrupt. Finally, in Section 5, we study the laminar phase length as a function of ϵ. Conclusions are given in Section 6.

2. The driven Double Scroll Circuit

The circuit is schematically shown in Fig. 1. It is composed by two capacitors, C_1 and C_2, two resistors, R and r, one inductor, L, and the non-linear resistor, R_{NL}.

The electronic value components used in our experiment are

$$C_1 = 0.0052\,\mu\mathrm{F}, \qquad C_2 = 0.056\,\mu\mathrm{F}, \qquad R = 1470\,\Omega, \qquad L = 9.2\,\mathrm{mH}, \qquad r = 10\,\Omega \tag{1}$$

and the driven force applied to the circuit can be represented by

$$q(t) = V \sin(2\pi f t) \tag{2}$$

where V is the amplitude and f is the frequency. The R_{NL} characteristic curve can be seen in Fig. 2 and is

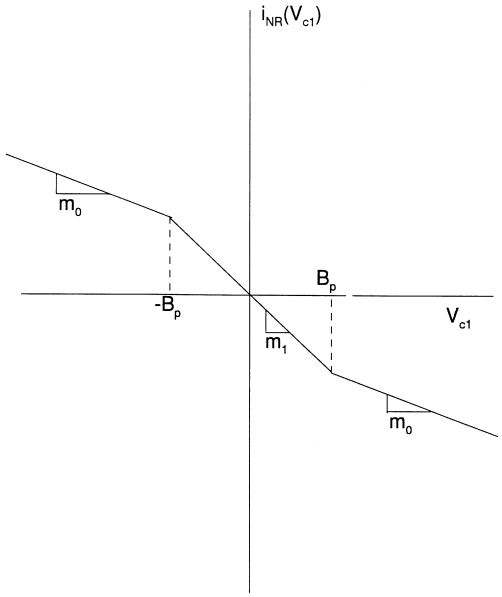

Fig. 2. The characteristic curve of the non-linear resistor R_{NL}.

mathematically represented by

$$i_{NR}(V_{C1}) = m_0 V_{C1} + 0.5(m_1 - m_0)|V_{C1} + B_p| + 0.5(m_0 - m_1)|V_{C1} - B_p|. \tag{3}$$

We can simulate the circuit of Fig. 1 by applying Kirchhoff's laws. So, the resulting state equations are

$$C_1 \frac{\mathrm{d}V_{C1}}{\mathrm{d}t} = \frac{1}{R}(V_{C2} - V_{C1}) - i_{NR}(V_{C1}), \quad C_2 \frac{\mathrm{d}V_{C2}}{\mathrm{d}t} = \frac{1}{R}(V_{C1} - V_{C2}) + i_L, \quad L\frac{\mathrm{d}i_L}{\mathrm{d}t} = -V_{C2} - q(t) \tag{4}$$

where V_{C1} and V_{C2} are the voltage across the capacitors C_1 and C_2, respectively, and i_L is the electric current across the inductor L. To avoid numerical problems we do not use the real component values in Eqs. (4) but a rescaled set of parameters given in terms of the real values. Thus, the parameters used in Eqs. (4) for doing numerical simulation of the circuit in Fig. 1 are

$$\frac{1}{C_1} = 10.0, \quad \frac{1}{C_2} = 1.0, \quad \frac{1}{L} = 6.0, \quad \frac{1}{R} = 0.6, \quad m_0 = -0.5, \quad m_1 = -0.8, \quad B_p = 1.0. \tag{5}$$

For the electronic components in Eq. (1), or the parameter simulation values in Eq. (5), and for a null perturbing amplitude $V = 0$, the circuit behaves chaotically. As the circuit is dissipative its dynamic variables (V_{C1}, V_{C2}, and i_L) evolve on a chaotic attractor named Double Scroll.

3. The experimental two-frequency torus breakdown

When the driven force is turned on, that means $V \neq 0$, a new frequency is introduced in the characteristic oscillations of the Double Scroll Circuit. This new frequency is responsible for the appearance of a quasi-periodic movement on a two-frequency torus (T^2).

In Fig. 3, the oscillations in (A) correspond to a limit cycle just after a Hopf bifurcation. In (B) we identify a second Hopf bifurcation of this limit cycle creating a torus T^2. Increasing further the driven frequency, we show in (C) a two-frequency torus breaking through type-II intermittency as confirmed by numerical simulations.

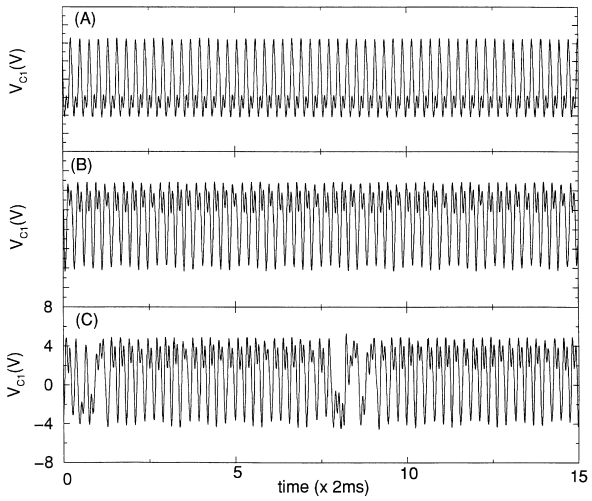

Fig. 3. Time evolution of the variable V_{C1} for a fixed amplitude $V = 0.700$ V and frequencies (A) $f = 1.852$ kHz, (B) $f = 1.923$ kHz and (C) $f \gtrapprox 1.923$ kHz.

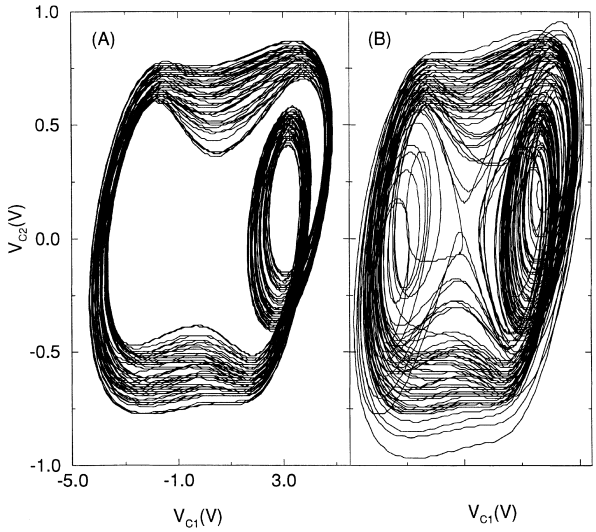

Fig. 4. Projection of the attractor on the variable space plane ($V_{C1} \times V_{C2}$) for (A) $f = 1.923$ kHz, and (B) $f \gtrsim 1.923$ kHz.

The bi-dimensional projection of the Double Scroll attractor on the plane ($V_{C1} \times V_{C2}$) for the parameters of Figs. 3(B,C) is shown in Fig. 4. In this figure, we see the torus T^2 (A) and its breakdown (B). After the breakdown the attractor grows in size and its trajectory evolves erratically all over this plane, eventually returning to the region where it was located the torus T^2 (the reinjection process), behaving regularly for a while, until it starts to evolve erratically again (the chaotic phase). This behavior is only observed in a two-frequency torus breakdown through the type-II intermittency.

To obtain the image of the torus T^2, one must analyze the crossings of the three-dimensional trajectory on a two-dimensional Poincaré section. However, as indicated in Fig. 1, we can only collect data from two channels. Therefore, only two dynamical variables are considered, $V_{C1}(t)$ and $V_{C2}(t)$. To obtain the three-dimensional attractor needed to visualize the torus T^2, we reconstruct the 3D chaotic attractor by using the time-delay method [19].

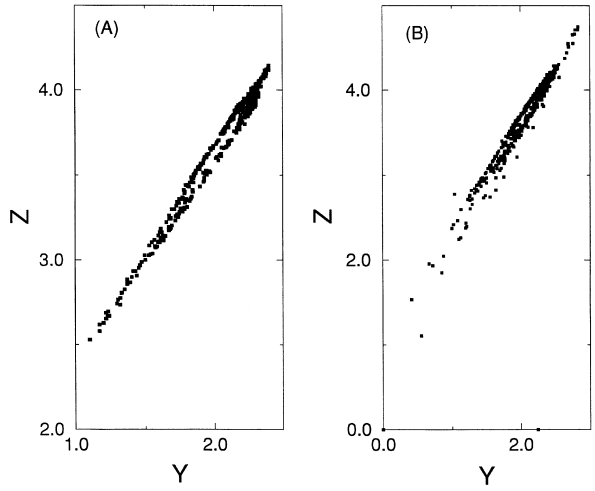

Fig. 5. (A) Poincaré section of the reconstructed quasi-periodic torus T^2 of the three-dimensional attractor obtained for $V = 0.700$ V and $f = 1.923$ kHz. (B) The torus T^2 breaks generating chaotic behavior for $V = 0.700$ V and $f \gtrapprox 1.923$ kHz. (A) and (B) have different axis scalings.

The considered dynamic variable is $V_{C1}(t)$ and the time-delay (time shift) rate is $p = 24\,\mu s$ (with the acquisition time $\delta = 2\mu s$). Thus, for a time series $V_{C1}(t)$, we construct a three-dimensional trajectory. The first point of this trajectory is $(V_{C1}(t), V_{C1}(t + p), V_{C1}(t + 2p))$, the second is $(V_{C1}(t + \delta), V_{C1}(t + \delta + p), V_{C1}(t + \delta + 2p))$, and so on. In this notation, the reconstructed trajectory has three coordinates represented by (X, Y, Z). Thus, the intersection of a reconstructed torus T^2 with the section $X = 0$ is shown in Fig. 5(A). The way chaos appears by torus breakdown is shown in Fig. 5(B). In the last figure, the characteristic chaotic bursts due to trajectory ejections (as analyzed in Section 4) can be already identified.

4. The simulated two-frequency torus breakdown

In the previous section, we describe the experimental onset of chaos through a two-frequency torus breakdown by analyzing the time evolution of the variables V_{C1} and V_{C2}, and also, by reconstructing the attractor. However, the data collected is not accurate enough to describe these transitions geometrically or more quantitatively. So, afterwards, the numerical experiment we show next has the purpose of establishing a scaling law for the laminar phase observed just after the appearance of chaos, and therefore a quantitative analysis for the transition observed in the experiment described before. In addition, even though the results shown experimentally were obtained by varying the driving frequency f, the same transition is also observed by varying the amplitude V.

Thus, in order to quantify the experimental results better, numerical work is presented by integrating Eqs. (4) with the parameters given by Eq. (5), for a fixed driven frequency $f = 0.18$. Thus, Fig. 6(A) shows a bifurcation diagram of the variable V_{C2}, when the trajectory crosses a Poincaré section at $V_{C1} = -1.5$, as a function of V. The abrupt appearance of chaos, seen in this figure, is confirmed by the first Lyapunov exponent λ (Fig. 6(B)). We have numerically determined that chaos first appears for $V_C = 0.2328691$ leading to $\lambda > 0$.

Comparing Fig. 7 with Fig. 4, one can realize similarities between the break of the torus, we see experimentally and the same phenomenon we see numerically. In Fig. 7(A), we see a projection of the attractor in the $V_{C1} \times V_{C2}$ space for a parameter smaller than the one when the torus breakdown occurs, for $V = 0.23285$, and in Fig. 7(B), we see the attractor when there is no torus T^2 any more, and type-II intermittency is present, for $V = 0.23290$.

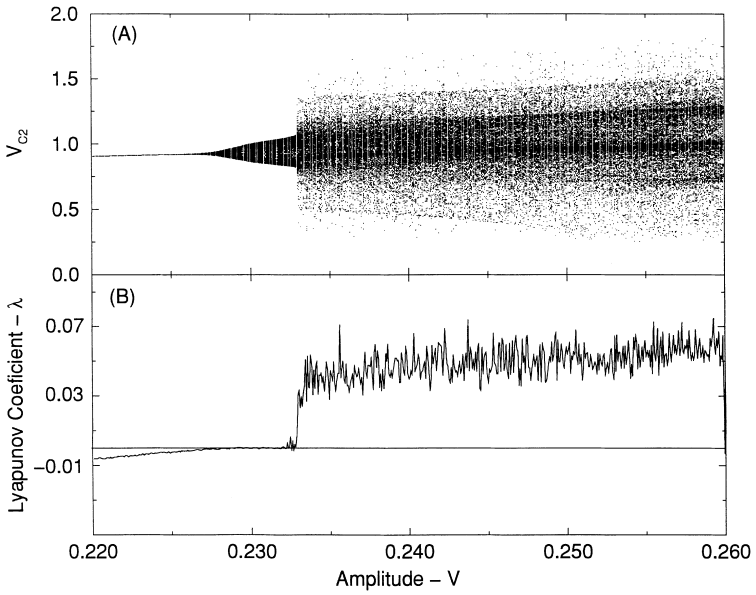

Fig. 6. (A) A bifurcation diagram showing the two-frequency torus creation (via Hopf bifurcation) and then its destruction, generating chaotic behavior, by a rising amplitude V and a fixed driving frequency $f = 0.18$. (B) The first Lyapunov exponent λ, for the same parameters of (A). That means chaos for $\lambda > 0$. $V_{C1} = -1.5$.

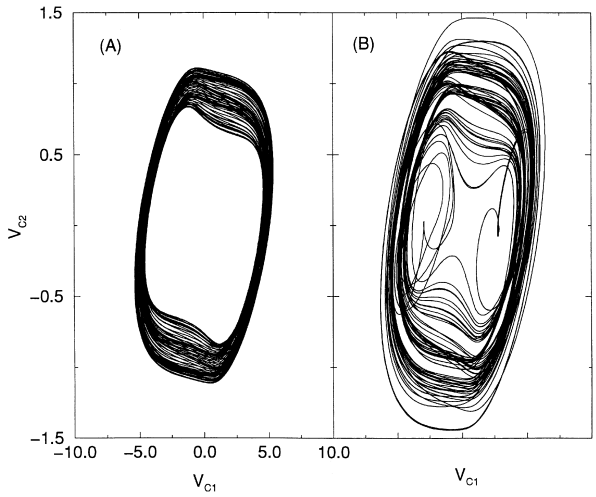

Fig. 7. Projection of the attractor on the variable space plane ($V_{C1} \times V_{C2}$) for $f = 0.18$ and (A) $V = 0.23285$, and (B) $V = 0.23290$.

In Fig. 8, we see a sequence of three figures showing the attractor through the Poincaré section positioned at $V_{C1} = -1.5$. So, in this figure, we see the attractor through the variables V_{C2} and i_L.

The torus T^2 is created after a supercritical Hopf bifurcation. In this situation, before the onset of chaos, the torus is a deformed circle with no folds or cuspids, as shown in Fig. 8(A) ($V = 0.2280000$). However, on rising the amplitude ($V = 0.2328690$), the torus T^2 folds in five parts resembling a five-sided polygon (Fig. 8(B)). The torus breaks as in Fig. 8(C) ($V = 0.2328691$) leading to the appearance of type-II intermittency, that causes the trajectory to evolve spirally around the previously existing repelling focus point, indicated in figure by o. So, we can say that the critical parameter is $V_C = 0.2328690$.

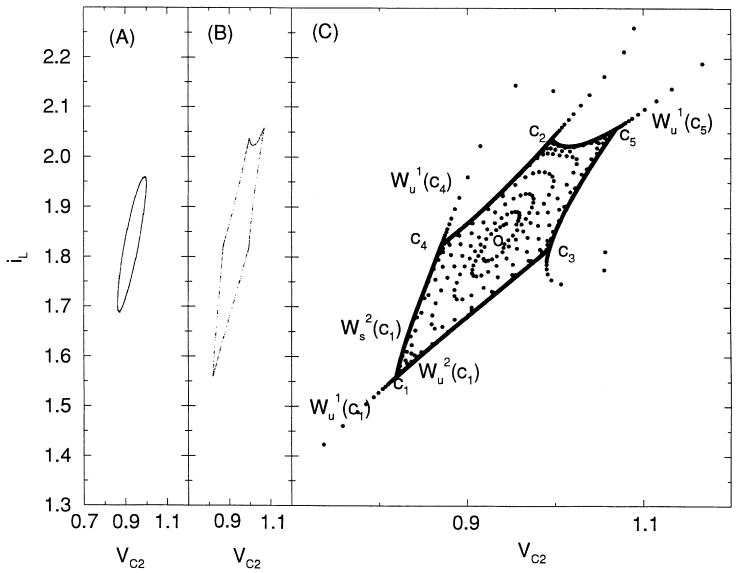

Fig. 8. (A) A quasi-periodic torus T^2 for $V = 0.2300000$. (B) The five-sided quasi-periodic folded torus for the critical parameter $V = 0.2328690$. (C) The destruction of the torus leading to a type-II intermittency. $V_{C1} = -1.5$.

Along the torus, not yet destroyed, a quasi-periodic trajectory is non-clockwise oriented with a winding number near the rational fraction $w = 3/5$. Three is the number of the trajectory rotations along the torus to return back to the same point, taking five complete cycles. It means that, after passing nearby a saddle point of Fig. 8, the trajectory crosses this Poincaré section five times before returning to the same saddle point. We can consider the flow on this section as a mapping G. So if c_n with $n = 1, \ldots, 5$, are the saddle points, then $G^5(c_n) = c_n$ and $G(c_n) = c_{n+1}$.

As a matter of fact, the laminar spiral trajectory is a five-spiral trajectory, which means that the trajectory visits one of the five spirals each time. These spirals evolve approaching asymptotically the previous stable five-sided polygon torus. In fact, each spiral tends to one of the five corners of the polygon. These corners, indicated by c_n, are saddle points with two different unstable manifolds. Along one unstable manifold, the trajectory is ejected outside the polygon causing the chaotic burst. Along the other, the trajectory is directed to the nearest saddle point in the non-clockwise direction (sampling each five steps in the Poincaré section). That means that $G.G^5(c_n)$ tends to c_{n+1}.

In Fig. 8(C), some points along the unstable manifolds responsible for the chaotic burst are indicated by W_{u}^1, and those responsible for the homoclinic saddle connection (an orbit in G^5 that connects the five saddle points) by W_{u}^2. So, we see that the unstable manifold of the saddle point c_1, $W_{\mathrm{u}}^2(c_1)$ is the stable manifold of the c_3, $W_{\mathrm{s}}^2(c_3)$.

We will not go into details about the chaotic burst. It is enough, for now, to say that the trajectory approaches the saddle points spiraling, is expelled from the broken torus along W_{u}^1, and then is reinjected back inside the broken torus (into the focus) leading again to the spiral laminar phase.

5. Analysis of the laminar length

We consider as laminar phase the regular behavior. However, as mentioned before, the trajectories shown in Fig. 8(C) stay for a while in the saddle points before they are ejected out of the broken torus. So, the laminar phase is due to the spiraling behavior caused by the repelling focus, located at the origin, plus the permanency of the trajectory in the vicinity of the saddle points.

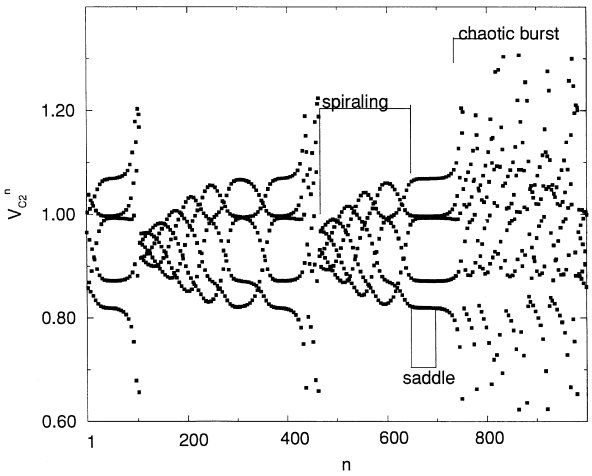

Fig. 9. Evolution of the variable V_{C2} through the section $V_{C1} = -1.5$ showing the laminar length composed by the spiraling behavior plus the permanency in the saddle point.

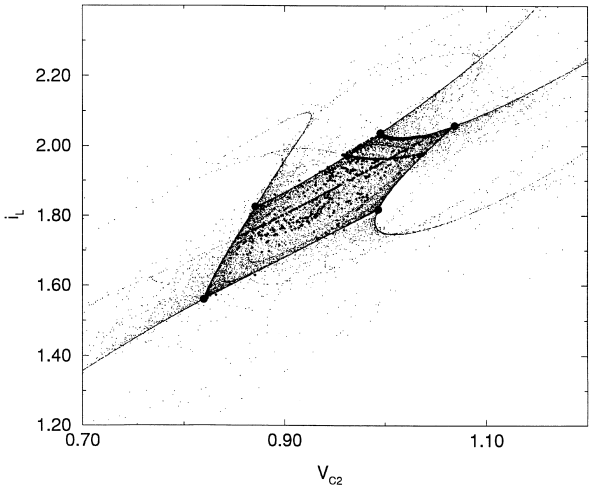

Fig. 10. The destroyed torus obtained for $f = 0.18$ and $V = 0.2328750$, where we can identify the first points to re-enter the focus (filled squares), and the saddle points (filled circles). $V_{C1} = -1.5$, and the number of steps $n = 200\,000$.

In Fig. 9, we show the evolution of the variable V_{C2}^n through the Poincaré section $V_{C1} = -1.5$, where the index n represents the nth time the trajectory crosses this section. In this figure, we see typical spiraling phases and permanency in the saddle points, followed by chaotic bursts, with the trajectory ejected along the unstable manifold of the saddle points.

In Fig. 9, we see that the permanency in the saddle point is shorter than the spiraling behavior. In fact, for a rising amplitude close to the critical value, both the spiraling length and the saddle permanency decrease. As we shall see, there is a competition behavior between these two regular phases.

For numerical analysis, we consider that a point on the Poincaré section belongs to a laminar trajectory if it is within a polygon encompassed by a closed curve that contains the five saddle points (plotted with a filled closed line in Fig. 10), or within circumferences of radius $\rho = 0.005$ centered in the saddle points. Naturally, the saddle permanence (S_P) is the number of steps the trajectory spends inside these circumferences. Therefore, if we call the

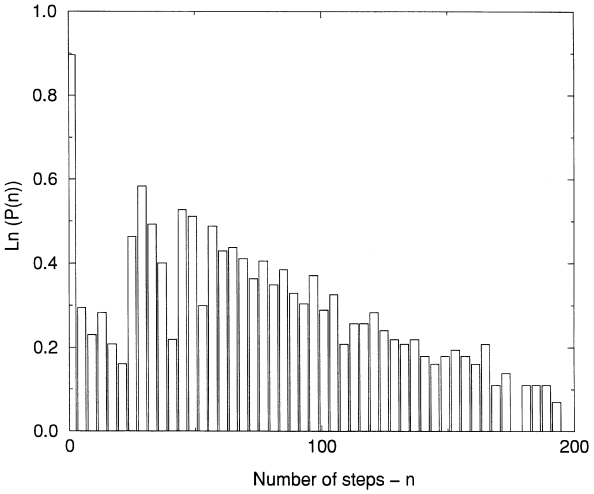

Fig. 11. Probability distribution $P(n)$ for the laminar length (the spiraling length plus the saddle permanence). The number of steps $n = 200\,000$. For the main peak $P(n) \approx 7000$.

length of the laminar phase as L_P, and the spiraling length as S_L,

$$S_L = L_P - S_P. \tag{6}$$

Pomeau and Manneville [6] considered a randomly and spatial uniform reinjection in the repelling focus to derive their logarithmic scaling law for the laminar (spiraling) phase. Richetti et al. [12] obtained a power scaling law for the laminar (spiraling) behavior for a unidimensional spatial reinjection. In the driven Double Scroll Circuit we find that the reinjection process due to the homoclinic saddle connection puts the trajectory in any part near the two-dimensional focus. However, the reinjection placement is not uniform as we can see in Fig. 10, where the squares indicating the first iterations around the focus (the re-entrance location) are mainly distributed along two main directions.

The two main directions on the re-entrance distribution (Fig. 10) cause the two-peaks observed in the laminar phase distribution $P(n)$ shown in Fig. 11 (where n is the number of times the trajectory crosses the Poincaré section during the laminar behavior). Each peak decays exponentially, $P(n) \propto \exp(-2\epsilon n)$, as determined by Pomeau and Manneville [6]. Here, $\epsilon = |V - V_c|$ and $V_c = 0.2328690$ is the critical amplitude for the torus breakdown. The main peak for small n represents the trajectories reinjected in the neighborhood of the saddle points and therefore quickly ejected. This is an evidence that there may exist a homoclinic trajectory through a saddle point, since the trajectory is biasymptotic to the basic cycle responsible for the saddle points, as we see on the Poincaré section [20].

We now show a new scaling law (distinct from the laminar (spiraling) length predicted by Pomeau and Manneville) considering the two regular phase lengths: S_P and L_P. Thus, Fig. 12 shows the saddle permanence, S_P, and the laminar phase length, L_P, indicated respectively by squares and circles, as a function of ϵ. We fitted these points and obtained that $S_P \propto \epsilon^{-\alpha}$, with $\alpha = 0.542 \pm 0.019$ (this function is represented by curve (3) in Fig. 12). The laminar phase behaves as $L_P = 1/(A + \beta\epsilon)$, with $\beta = 0.075 \pm 0.002$ and $A = 6 \times 10^{-5}$, for $\epsilon \geq 0.000011$ (curve (2)), and $L_P \propto \epsilon^{-\gamma}$, with $\gamma = 0.151 \pm 0.009$, for $\epsilon < 0.000011$ (curve (1) in Fig. 12).

Using Eq. (6), we calculated the spiraling length, S_L, from the numerical values obtained for S_P and L_P, as a function of ϵ. Thus, the spiraling average length, S_L, as a function of ϵ is shown in Fig. 13. We see that S_L increases for $\epsilon < 0.000011$, and decreases for $\epsilon \geq 0.000011$.

The fast variation of the spiraling length for $\epsilon < 0.000011$, therefore in a small neighborhood of the critical parameter, is due to the homoclinic saddle connection associated to the reinjection process.

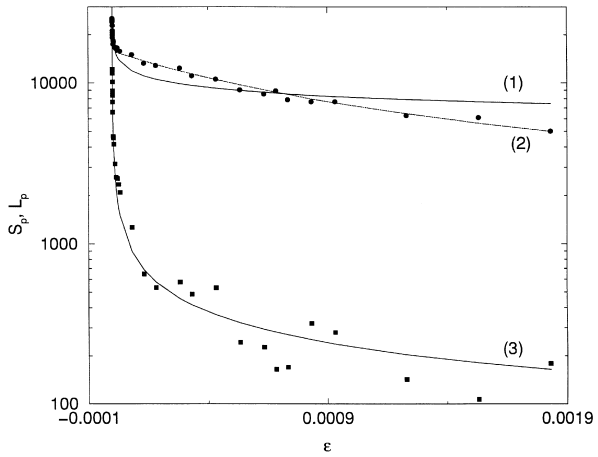

Fig. 12. Saddle permanence (squares) and the laminar phase length (circles) with respect to ϵ. The number of steps $n = 30\,000$. Curve (1) represents the laminar phase, $L_P \propto \epsilon^{\gamma}$, for $\epsilon < 0.000011$, and curve (2) the laminar phase, $L_P = 1/(A + \beta\epsilon)$, for $\epsilon \geq 0.000011$. Curve (3) represents the spiraling permanence $S_P \propto \epsilon^{\alpha}$. The vertical axis is in a logarithmic scale. $\epsilon = |V - V_c|$.

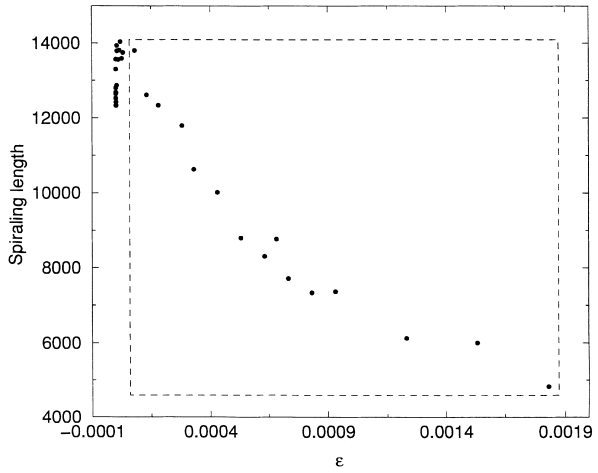

Fig. 13. Spiraling length, S_L, obtained through Eq. (6). The number of steps $n = 30\,000$. $\epsilon = |V - V_c|$.

Table 1
In this table S_L represents the spiraling length, L_P, the laminar phase, and S_P, the saddle permanence. The scaling coefficients are: $\alpha = 0.542 \pm 0.019$, $\gamma = 0.151 \pm 0.009$, $A = 6 \times 10^{-5}$, $\beta = 0.075 \pm 0.002$.

	$\epsilon < 0.000011$	$0.000011 \leq \epsilon < 0.0019$	$\epsilon \geq 0.0019$
S_L	–	$\ln(1/\epsilon)$	–
L_P	$\epsilon^{-\gamma}$	$1/(A + \beta\epsilon)$	$1/(A + \beta\epsilon)$
S_P	$\epsilon^{-\alpha}$	$\epsilon^{-\alpha}$	$\epsilon^{-\alpha}$

For $0.000011 < \epsilon < 0.001900$ (region indicated in the box of Fig. 13), the spiraling length, S_L, behaves as predicted theoretically by Pomeau and Manneville [6]. So, we also find a logarithmic scaling law, $S_L \propto \ln(1/\epsilon)$ as one can see in Fig. 14. Therefore, our results show that depending on what type of regular behavior (S_L, L_P, or S_P) we want to analyze, its length scales depend also on ϵ as shown in Table 1. In this table, we display the scaling laws for the three regular phase length, S_L, L_P, and S_P, with their respective scaling coefficients, as we change ϵ.

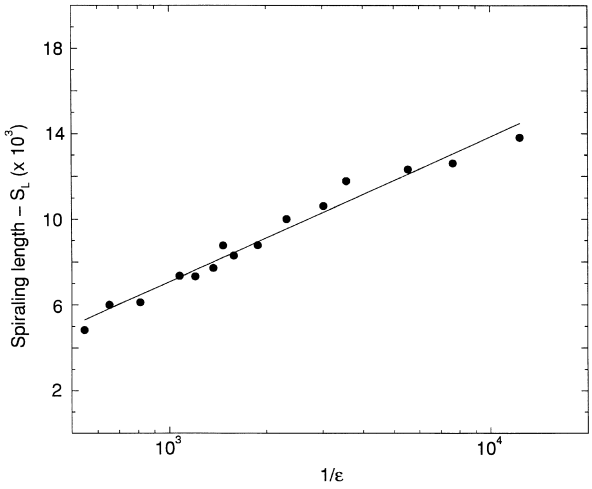

Fig. 14. The function S_L, obtained through Eq. (6). The abscissa axis is in a logarithmic scale and represents the inverse of ϵ. $\epsilon = |V - V_c|$.

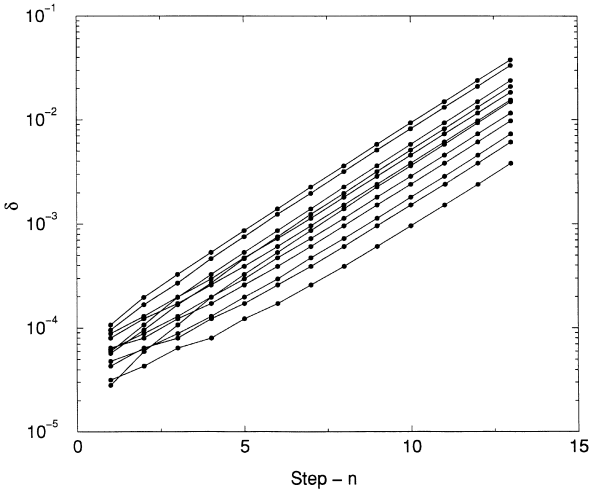

Fig. 15. The spatial relative distance δ between a sequence of points P of an ejected trajectory (in the neighborhood of the point c_2) and the saddle point c_2. The vertical axis is in a logarithmic scale.

For $\epsilon > 0.2340000$, there is a saddle disconnection bifurcation [18] and the spiraling behavior loses its original shape. Before the saddle disconnection, each of the five spirals would go spirally, around the origin, approaching the saddle points. After the saddle disconnection, this spiraling behavior becomes oriented and a point falling down in the previous stable focus is directed to the saddle point, without the present spiraling behavior.

The power scaling law for the saddle permanence (with $\alpha = -0.542$) may give us the wrong impression that this permanence would be due to a type-I intermittency. However, the saddle permanence can not be associated to such a phenomenon since, as pointed out in [20], as a consequence of the marginality of the basic cycle in the intermittent systems, the trajectories leave the cycle as $1/t^{\mu}$ for $t \to -\infty$ (with $\mu = 1$ for type-I intermittency) while the escape from the cycle in systems with a homoclinic tangency behaves like $e^{\alpha t}$ for $t \to -\infty$ (with $\alpha > 0$).

What we found in the neighborhood of the saddle points is that the trajectory is ejected from these points exponentially as we can see in Fig. 15. In this figure, we choose the saddle point c_2 in Fig. 8 and consider a

trajectory passing through a neighborhood δ of this saddle point. After the trajectory crosses the Poincaré section $V_{C1} = -1.5$ at the point $P = (V_{C2}, i_L)$, we analyze how δ grows up after n steps. So, for $n = 1$, we see the spatial displacement $\delta = G^5(P) - c_2$, and for $n = 2$, we see $\delta = G^5.G^5(P) - c_2$, and so on.

This result assures that the trajectory leaves the unstable manifold $W_u^2(c_2)$ with an exponentially spatial divergence. Furthermore, the unstable manifold W_u^1 has also an exponential divergence. We know that the junction of the manifolds W_u^2 form the homoclinic saddle connection. Following the same thought, it is natural to believe that from the unstable manifolds W_u^1 there may exist an orbit that leaves the basic cycle along $W_u^1(c_n)$ and returns to this cycle through the stable manifold $W_s(c_m)$ (note that $n \neq m$). If such an orbit exists, it is an orbit that is biasymptotic to a saddle point for $t \to \infty$ along the $W_s^2(c_m)$, and for $t \to -\infty$ along the $W_u^1(c_n)$. And this would be an homoclinic orbit that connects a saddle point with another (or the same) saddle point.

Following the same reasoning, it is also natural to believe that there might exist a heteroclinic orbit connecting the saddle points with the unstable focus, which is responsible for the reinjection process.

We numerically found at least two orbits that seem to behave like the homoclinic orbit, that connects the saddle points, and the heteroclinic orbit, that connects the saddle points with the unstable focus. They might be localized in the two extremes inside the basic cycle, and, due to their existence, the area inside the attractor of Fig. 4 is filled by trajectories.

The possible existence of these two main homoclinic and heteroclinic orbits could explain the two main directions for the trajectory reinjection in the focus.

A recent result obtained by doing several amplifications of Fig. 10 near the saddle points, shows that in the neighborhood of the saddle points there exists a Smale Horseshoe process [18], due to a transversal crossing of the manifolds evolved in the homoclinic saddle connection, around the saddle points.

6. Conclusions

In this work, we identify for the driven Double Scroll Circuit, the first global non-linear mechanism responsible for trajectory reinjections around a repelling focus, leading to the type-II intermittency. This mechanism is a homoclinic saddle connection that surrounds the repelling focus. Because of such a scenario, the considered laminar phase is the time the trajectory spends in the vicinity of the saddle points plus the spiraling length (the laminar phase considered by Pomeau and Manneville [6]) around the focus.

We have found that this new considered laminar phase, L_P, scales as $L_P \propto \epsilon^{\gamma}$, with $-\gamma = 0.151 \pm 0.009$, for $\epsilon < 0.000011$, and $L_P = 1/(A + \beta\epsilon)$, with $\beta = 0.075 \pm 0.002$ and $A = 6 \times 10^{-5}$, for $\epsilon \geq 0.000011$, $(\epsilon = |V - V_c|)$. If we consider a region for $\epsilon > 0.000011$, we found a logarithmic scale law for the spiraling length, S_L, as theoretically proposed by Pomeau and Manneville. The saddle permanence scales as $S_P \propto \epsilon^{-\alpha}$, with $\alpha = 0.542 \pm 0.019$.

Therefore, we see that depending on the way we analyze the regular phase, and the range of ϵ, different scaling laws are obtained. A result that confirms theoretical assumptions that the type-II intermittency is a non-generic bifurcation is in [9].

Although the trajectory reinjection is typically two-dimensional, the set of re-entry points is mainly distributed along two directions. This re-entrance causes the appearance of two peaks in the probability distribution for the laminar length. Each peak decays exponentially $P(n) \propto \exp(-2\epsilon n)$, as predicted by Pomeau and Manneville for a re-entrance model with a random uniform two-dimensional distribution. Besides these two peaks, there is one main peak that represents a trajectory reinjected along the stable manifold of a saddle point and quickly expelled along the unstable manifold. The existence of this peak is a strong evidence of the presence of a heteroclinic trajectory connecting the saddle points with the unstable focus.

The saddle permanence may be erroneously interpreted as the regular phase of a type-I intermittency because of its observed scaling power law. However, we have shown that the spatial escape along the unstable manifold of the

saddle points is exponential, typical of homoclinic tangencies, one more evidence of the existence of a homoclinic trajectory to the saddle points.

We have numerically found two orbits that seems to behave as a homoclinic orbit to the saddle points. If such orbits exist in its neighborhood there is a Smale Horseshoe process that would be the reason for the reinjection process. Naturally, the neighborhood of this orbit belongs to the vicinity of the repelling focus and so the reinjection process is explained.

Acknowledgements

The authors thank Mr. A.P. Reis for the assistance in the electronic apparatus, Dr. A.N. Fagundes for making the codes for the data acquisition, and for useful computation advices, the computational assistance of Dr. W.P. de Sá, and Dr. J.C. Sartorelli for its useful experimental advices and the assistance in the experimental work. We also thank Dr. K. Ullmann for his useful suggestions. This work was partially supported by FAPESP and CNPq.

References

[1] T. Matsumoto, L.O. Chua, IEEE Trans. Circuits Syst. CAS-32 (1985) 797.
[2] M. Itoh, H. Murakami, L.O. Chua, Int. J. Bifurcation and Chaos 4 (1994) 1721.
[3] K. Murali, M. Lakshmanan, Int. J. Bifurcation and Chaos 2 (1992) 621.
[4] L. Pivka, A.L. Zheleznyak, L.O. Chua, Int. J. Bifurcation and Chaos 4 (1994) 1743.
[5] K. Murali, M. Lakshmanan, Int. J. Bifurcation and Chaos 1 (1991) 369.
[6] Y. Pomeau, P. Manneville, Phys. Lett. A 79 (1980) 33.
[7] Y. Pomeau, P. Manneville, Commun. Math. Phys. 74 (1980) 189.
[8] G.J. de Valcárcel, E. Roldán, Víctor Espinosa, R. Vilaseca, Phys. Lett. A 206 (1995) 359.
[9] A.J. Lichtenberg, M.A. Lieberman, Regular and Chaotic Dynamics, Springer, New York, 1992.
[10] M.S. Baptista, I.L. Caldas, Chaos, Solitons, and Fractals 7 (1996) 325.
[11] T. Kawabe, Y. Kondo, M. Tanaka, Progr. Theor. Phys. 96 (1996) 1.
[12] P. Richetti, F. Argoul, A. Arneodo, Phys. Rev. A 34 (1986) 726.
[13] L.P. Shil'nikov, Int. J. Bifurcation and Chaos 4 (1994) 489.
[14] J. San-Martín, J.C. Antoranz, Phys. Lett. A 219 (1996) 69.
[15] A. Lahiri, T. Nag, Phys. Rev. Lett. 62 (1989) 1933.
[16] J.-Y. Huang, J.-J. Kim, Phys. Rev. A 36 (1987) 1495.
[17] J. Sacher, W. Elsässer, E.O. Göbel, Phys. Rev. Lett. 63 (1989) 2224.
[18] D.K. Arrowsmith, C.M. Place, An Introduction to Dynamical Systems, Cambridge University Press, Cambridge, 1990.
[19] F. Takens, Dynamical Systems and Turbulence, Springer, Berlin, 1980.
[20] P. Gaspar, X.-J. Wang, J. Stat. Phys. 48 (1987) 151.